sustainability

MDPI

Article

Calibration of Turbulent Model Constants Based on Experimental Data Assimilation: Numerical Prediction of Subsonic Jet Flow Characteristics

Xin He [1], Changjiang Yuan [1], Haoran Gao [2], Yaqing Chen [3,*] and Rui Zhao [1]

[1] School of Air Traffic Management, Civil Aviation Flight University of China, Guanghan 618307, China; hexin513@sina.com (X.H.)
[2] Institute Office, Civil Aviation Flight University of China, Guanghan 618307, China
[3] CAAC Key Laboratory of Flight Technology and Safety, Civil Aviation Flight University of China, Guanghan 618307, China
* Correspondence: chenyaqingmail@sina.com

Abstract: Experimental measurements and numerical simulations are two primary methods for studying turbulence. However, these methods often struggle to balance the accuracy and breadth of results. In order to accurately predict the flow characteristics of subsonic jet exhaust and provide a research foundation for the runway crossing operation after the takeoff point, this study utilizes the ensemble Kalman filter algorithm to recalibrate the SA turbulence model constants by integrating NASA's experimental particle image velocimetry (PIV) data with a sample library generated using Latin hypercube sampling to obtain corresponding flow field calculations. The modified model constants effectively improve the prediction of jet flow characteristics, reducing the spatially averaged relative error along the horizontal axis behind the nozzle from 13.04% to 4.6%. This study focuses on enhancing the accuracy of numerical predictions for subsonic jet flows via the adjustment of turbulence model constants. The recalibrated model constants are then validated to improve the prediction of jet flows under various conditions. The findings have important implications for acquiring high-fidelity data on rear engine jet flows after takeoff, enabling precise determination of safety separation distances, and enhancing the operational efficiency of airports.

Keywords: turbulence; jet flow; numerical simulation; data assimilation; ensemble Kalman filter

Citation: He, X.; Yuan, C.; Gao, H.; Chen, Y.; Zhao, R. Calibration of Turbulent Model Constants Based on Experimental Data Assimilation: Numerical Prediction of Subsonic Jet Flow Characteristics. *Sustainability* **2023**, *15*, 10219. https://doi.org/10.3390/su151310219

Academic Editors: Feng Xiang, Meng Zhang and Ying Zuo

Received: 1 June 2023
Revised: 20 June 2023
Accepted: 26 June 2023
Published: 27 June 2023

1. Introduction

To enhance airport operational efficiency, alleviate operational pressure, and reduce unsafe incidents such as runway incursions, Chen et al. [1] proposed a runway crossing operation mode behind the takeoff point. The runway crossing operation behind the takeoff point involves departing an aircraft utilizing a non-full runway takeoff, crossing the runway from behind the takeoff point while maintaining a certain safety clearance, and entering a designated taxiway or runway. In this crossing mode, the impact of subsonic jet exhaust generated by preceding aircraft on subsequent aircraft becomes particularly significant, posing a challenge in obtaining accurate data on the preceding jet exhaust. In the civil aviation domain, subsonic jet nozzles are widely used in aircraft engines, providing high thrust efficiency, reducing noise and emissions, and demonstrating excellent fuel efficiency and environmental performance. The precise prediction of the flow characteristics and evolution of subsonic jet exhaust plays a crucial role in determining the crossing intervals for the runway crossing operation behind the takeoff point.

Uzun et al. have numerically simulated circular jet flow using Large Eddy Simulation (LES) coupled with the Ffowcs Williams–Hawkings method [2]. Xie et al. have conducted an experimental study and numerical simulation to investigate the flow field characteristics and influencing factors of subsonic jets [3]. Manovski has used the multiple-pulse Shake-The-Box technique for three-dimensional Lagrangian particle tracking of subsonic jet flow, demonstrating its application in high-precision flow field measurement and research [4]. Yang et al. investigated the turbulence characteristics of the cavitation cloud in submerged cavitating jet flows under high Reynolds number conditions and conducted a detailed analysis using experimental measurement methods [5]. Zhang et al. studied the flow field characteristics of water jet nozzles and conducted a detailed measurement and analysis of the flow behavior of the jet using experimental methods, revealing the flow field structure and turbulence characteristics of the jet [6]. He et al. conducted research on the influence distance of subsonic engine jets using an improved Delayed Detached Eddy Simulation (DES) method and the Spalart–Allmaras (SA) turbulence model. They obtained the influence distance of the engine jets and performed analysis and evaluation of the obtained results [7]. It can be observed that experimental measurements and numerical simulations are currently the two main approaches for studying turbulent flow in jet flows. However, these two methods often have certain limitations. In terms of experimental measurements, the measurement range is often constrained via the measurement hardware, and there are difficulties in conducting measurements in areas with complex boundaries or internal measurement structure obstructions. In the field of numerical simulations, high-precision methods such as DNS and LES provide complete spatiotemporal information, but they suffer from significant computational costs, making their industrial applications challenging. Reynolds-averaged Navier–Stokes (RANS) methods, with relatively lower computational requirements, are the mainstream tools for industrial numerical simulations. However, they are also subject to uncertainties associated with model constants [8,9]. Therefore, the aforementioned approaches are subject to their respective limitations, and they cannot effectively balance the accuracy and comprehensiveness of the results [10]. In recent years, the data assimilation method (DA), widely used in disciplines such as atmospheric forecasting and oceanic hydrology, has been introduced into the field of fluid mechanics, offering a new approach to turbulent flow research. In the era of big data, data assimilation methods can combine the advantages of both experimental measurements and numerical simulations to obtain high-fidelity data for turbulence and broaden their application prospects in engineering. Thus, DA has the potential to overcome the limitations of traditional methods and achieve a better balance between accuracy and breadth of results [11].

To improve the accuracy and broaden the application prospects of turbulent flow research, significant efforts have been made to combine experimental data with simulations. Margheri studied the uncertainty of constants in different RANS models using data assimilation methods, and their results showed that compared to the k-ω SST model, the sensitivity of predicted parameters to constant values in the k-ε model was higher [12]. Kato proposed using ensemble transform Kalman filtering to assimilate experimental pressure distribution data as observation values, reducing uncertainties in state variables and improving the turbulent flow field [13]. Zhang et al. proposed the Regularized Ensemble Kalman Filter (REnKF) method, which integrated various heterogeneous data to reconstruct turbulent information and significantly improved the accuracy of turbulent reconstruction [14]. Li et al. proposed the D-DARK method, which used a data-driven approach to set target cost functions for the k-ω model in RANS methods, and used a gradient descent-like method to obtain optimal model constants [15]. Gallo conducted turbulent numerical optimization of the blade profile for the Savonius-type rotor and employed response surface methodology to enhance the performance and efficiency of the rotor [16]. Mi et al. investigated the hydraulic characteristics of a continuous submerged jet on a wall using numerical simulation and PIV experiments [17]. Deng used PIV flow field measurement data to estimate optimal constants for various turbulent models using the EnKF method and demonstrated that using improved turbulent models with optimal constants significantly improved flow field reconstruction [18].

Although extensive research has been conducted by scholars in relevant fields, studies on data assimilation for subsonic jet flow remain relatively limited, and there is a lack of research on the generalization capability of assimilated turbulence models. In this study, the model constants are recalibrated via EnKF data assimilation and applied to jet flow under different conditions to verify the effectiveness of assimilation. Due to the semi-empirical nature of the turbulent models commonly used in Reynolds-averaged Navier–Stokes (RANS) methods, which involve the incorporation of numerous engineering empirical constants, their respective applications are characterized by the limited applicability and poor capability to represent complex turbulence phenomena. Therefore, in order to enhance the predictive accuracy of numerical simulations for the flow characteristics of subsonic jets and to provide new research methods and approaches for the operating mode of crossing the runway after the takeoff point, this study focuses on the NASA subsonic axisymmetric jet model. The Spalart–Allmaras (SA) model is employed for numerical simulations, and Ensemble Kalman Filtering (EnKF) data assimilation is performed using velocity distribution data obtained from experimental measurements conducted with Particle Image Velocimetry (PIV) techniques [19,20] employed by NASA. Finally, the relevant validations, comparison of flow field parameters, and analysis are conducted to assess the degree of improvement in the predictive performance of the SA model after calibration and its applicability to jet flow under different conditions.

2. Mathematical Principles

2.1. Turbulence Model Equations

Reynolds-averaged Navier–Stokes (RANS) models have gained significant traction in the field of numerical turbulence simulation owing to their computational efficiency and low hardware requirements. The Spalart–Allmaras (SA) one-equation turbulence model, in particular, has emerged as a widely preferred option in engineering thanks to its reliability, high accuracy, and excellent convergence [21]. Nevertheless, owing to the inherent uncertainties associated with the model, there may exist certain discrepancies between the numerical predictions of jet flow and the outcomes obtained from high-precision experimental measurements. However, due to the inherent uncertainty factors in the model itself, the numerical predictions of jet flows using these models may introduce certain errors compared to high-precision experimental measurements. The standard one-equation S-A model solves for the working variable $\hat{v}$ based on the assumption of turbulent viscosity, which is governed by the following transport equation:

$$\frac{\partial \hat{v}}{\partial t} + u_j \frac{\partial \hat{v}}{\partial x_j} = c_{b1}(1 - f_{t2})\hat{S}\hat{v} - \left[c_{\omega 1} f_\omega - \frac{c_{b1}}{\kappa^2} f_{t2}\right]\left(\frac{\hat{v}}{d}\right)^2 + \frac{1}{\sigma}\left[\frac{\partial}{\partial x_j}\left((v + \hat{v})\frac{\partial \hat{v}}{\partial x_j}\right) + c_{b2}\frac{\partial \hat{v}}{\partial x_i}\frac{\partial \hat{v}}{\partial x_i}\right] \tag{1}$$

The vortex viscosity coefficient μ_t can be calculated as follows:

$$\mu_t = \rho \hat{v} f_{v1} \tag{2}$$

where

$$f_{v1} = \frac{\chi^3}{\chi^3 + c_{v1}^3}$$

$$\chi = \frac{\widetilde{v}}{v}$$

ρ represents fluid density; $v = \frac{\mu}{\rho}$ represents the dynamic viscosity coefficient; μ represents the molecular kinetic viscosity coefficient; f is a function of turbulent viscosity ratio χ.

The definitions of other various constants and variable functions in the equation are as follows:

$$\hat{S} = \Omega + \frac{\hat{v}}{\kappa^2 d^2} f_{v2}$$

where $\hat{S}$ represents the corrected vorticity intensity; $\Omega = \sqrt{2W_{ij}W_{ij}}$ represents the vorticity intensity; κ represents the Karman constant; d represents the distance between the point in the field and the surface of the object, where

$$f_{v2} = 1 - \frac{\chi}{1+\chi f_{v1}},\ f_w = g\left[\frac{1+c_{w3}^6}{g^6+c_{w3}^6}\right]^{1/6}$$

$$g = r + c_{w2}\left(r^6 - r\right)$$

$$r = \min\left\{\frac{\hat{v}}{\hat{S}\kappa^2 d^2}, 10\right\}$$

$$f_{t2} = c_{t3} \cdot e^{-C_{t4}\chi^2}$$

$$W_{ij} = \frac{1}{2}\left(\frac{\partial u_i}{\partial x_j} - \frac{\partial u_j}{\partial x_i}\right)$$

In the Fluent 2020 R2 software, the six model constants included in the SA turbulence model are provided as the subject of investigation, and their default values are presented in Table 1.

Table 1. Default values of SA model constants.

Constants	c_{v1}	c_{b1}	c_{b2}	c_{w2}	c_{w3}	σ
Default Value	7.1	0.1355	0.622	0.3	2.0	2/3

2.2. Data Assimilation

The data assimilation process is essentially an inversion process, where the form of the prediction model establishes the mapping relationship between the prediction parameters and the model constants (prediction). Data assimilation utilizes a certain algorithm (assimilation algorithm) to analyze the mapping relationship (analysis) and comprehensively synthesize relevant measurement data (observation) to infer and calibrate model constants (update). The three main elements of the process are the prediction model, observation data, and the assimilation algorithm. There are many algorithms used in data assimilation, including three-dimensional variational, four-dimensional variational, particle filtering, extended Kalman filtering, ensemble Kalman filtering, and ensemble transform Kalman filtering. For variational methods, it usually relies heavily on highly complex system model adjoint equations to minimize the cost function, which is not suitable for optimizing complex models [22]. Particle filtering uses a large number of random samples for the search in the state space, which can lead to excessive computational costs and a waste of resources on useless particles. Compared to these methods, Kalman filter-based assimilation methods are easier to implement, as they can flexibly adapt to different models by obtaining prior statistical information about the numerical models. Among them, the ensemble Kalman filter algorithm is one of the most commonly used algorithms in this type of assimilation method, which was proposed by Evensen in 1994 [23]. The algorithm has been developed based on the classical Kalman filter and the extended Kalman filter algorithms, and it can modify the prediction model by combining observational data. Furthermore, related studies have indicated that for optimizing turbulent numerical models, the optimization performance of the ensemble Kalman filtering is superior to that of the ensemble transform Kalman filtering [24]. Therefore, this study employs the Ensemble Kalman Filter algorithm as the assimilation method.

2.2.1. Ensemble Kalman Filter

The Kalman filter is a statistical filter [25] commonly used to filter noise in signals with white noise and obtain useful information. Kalman introduced discrete Kalman filtering for discrete systems in 1960 and, in the following year, collaborated with Bucy to extend it to continuous-time systems. Kalman filtering is a recursive data processing method widely applied to discrete linear system states with white Gaussian noise. The basic idea of Kalman filtering is to first obtain a background field using a model, then incorporate new observations and use the theory of minimum variance estimation to re-estimate the model state, aiming to obtain analysis results with the minimum error variance [26].

The Ensemble Kalman Filter (EnKF) algorithm is a powerful data assimilation method that combines Kalman filtering with ensemble forecasting. The method estimates the covariance between the state and observation variables by using the results of the ensemble forecast. The analysis is then updated by incorporating observation data and covariance, and the ensemble is re-analyzed and forecasted accordingly [27]. EnKF is a widely used data assimilation method that effectively addresses the assimilation problem in nonlinear models [28]. Specifically, in optimizing numerical models for turbulence with high-order nonlinearity, EnKF targets the following nonlinear system:

$$x_f = F(x_0, v) \tag{3}$$

$$y = Hx_f + w \tag{4}$$

where Equation (3) is the predictive equation of a high-order nonlinear system, and Equation (4) is the observation equation. In these equations, x_f is the prediction of the system state parameters, y is the observation, x_0 is the initial state of the system, v and w are the noise of the system and observation, F is the prediction model, and H is the observation function.

The main processes of the algorithm include the prediction process and analysis process.

In the first step of the ensemble Kalman filter algorithm, referred to as the prediction process, the state parameter vectors of each member in the ensemble set are calculated using the SA turbulence model. Starting from the initial state, the numerical simulation for turbulence is performed until convergence is achieved. The state parameters are obtained by applying Formula (5), which is expressed as follows:

$$x_f^i = F\left(x_0^i, v^i\right) \tag{5}$$

In this study, the prediction model F is represented by the SA model equation, where the state parameters of the ensemble members are denoted by $x_f^i = \begin{pmatrix} q^i \\ \theta^i \end{pmatrix} = \left(q_1^i, q_2^i, \ldots, q_n^i, \theta^i\right)^T$, q^i represents the flow velocity of the uniformly distributed jet in the horizontal axis direction behind the nozzle for the i-th prediction in the ensemble, and $\theta = (c_{v1}, c_{b1}, c_{b2}, c_{w2}, c_{w3})$ is the constant vector for the turbulent model. In the SA model, σ is considered to have a certain degree of universality owing to its correlation with the Prandtl number [29]; hence, the value of σ is not taken into account.

The average value of the set members is determined by Equation (6), which is expressed as follows:

$$\overline{x}_f = \frac{1}{l}\sum_{i=1}^{l} x_f^i \tag{6}$$

where the superscript i represents the index of set elements, l represents the total number of set members, and $\overline{x}_f$ represents the mean value of set members, respectively.

The second step is the analytical process, which constitutes the core of the Ensemble Kalman filtering algorithm. This step determines the Kalman gain and updates ensemble members by integrating the uncertainty of observation information and statistical information of ensemble members [25]. The process of this step is as follows:

(1) Analysis of prediction errors

$$P = \frac{1}{t-1}\sum_{i=1}^{l}\left(x_f^i - \overline{x}_f\right)\left(x_f^i - \overline{x}_f\right)^T \tag{7}$$

$$R = \frac{1}{l-1}WW^T \tag{8}$$

where

$$W = \begin{pmatrix} w^1, & w^2, & \cdots & w^l \end{pmatrix} \tag{9}$$

(2) Kalman gain calculation

$$K = PH^{\mathrm{T}}\left(HPH^{\mathrm{T}} + R\right)^{-1} \tag{10}$$

(3) Updating ensemble members

$$x_{\mathrm{a}}^i = x_f^i + K\left(y_{\exp} + w^i - Hx_f^i\right) \tag{11}$$

The mean value of the corresponding new set members is calculated as follows:

$$\overline{x_a} = \frac{1}{l}\sum_{i=1}^{l} x_a^i \tag{12}$$

For highly nonlinear models, a single iteration of the analytical process after the prediction step is often insufficient to achieve relatively accurate predictions. Therefore, this study performed multiple iterations of the Ensemble Kalman filtering algorithm for the prediction and analytical processes, as shown in Figure 1. The algorithm determines convergence when the standard deviation of ensemble members is less than 10^{-5} or when the maximum number of iterations (10,000) is reached [30].

2.2.2. Model Constant Calibration

The calibration of model constants in this paper is based on the data assimilation method of Ensemble Kalman filtering. The state matrix of the ensemble is defined as follows:

$$X = \begin{pmatrix} x_f^1, & x_f^2, & \cdots & x_f^l \end{pmatrix} = \begin{bmatrix} q_1^1 & q_1^2 & q_1^3 & \cdots & q_1^l \\ q_2^1 & q_2^2 & q_2^3 & \cdots & q_2^l \\ \cdots & \cdots & \cdots & \cdots & \cdots \\ q_n^1 & q_n^2 & q_n^3 & \cdots & q_n^l \\ \theta_1 & \theta_2 & \theta_3 & \cdots & \theta_l \end{bmatrix}_{k\times l} = \begin{pmatrix} Q \\ \theta \end{pmatrix} \tag{13}$$

Here, q_j^i represents the predicted velocity at the j-th point corresponding to the i-th ensemble member in the flow field computed using the RANS model. Θ denotes the undetermined RANS model constants, k represents the number of state variables, and l represents the total number of ensemble members.

The observed experimental velocity data is expressed as follows:

$$y_{\exp} = \widetilde{q}_i = (\widetilde{q}_1, \widetilde{q}_2, \ldots, \widetilde{q}_n)^T \tag{14}$$

where $\widetilde{q}_i$ represents the experimentally measured velocities at different locations, and n represents the number of measurement points.

The assimilation observation matrix Y is defined as follows:

$$Y = \left(y^1, y^2, \ldots, y^l\right)_{n\times l} = y_{\exp}1_{1\times n} + W = \begin{bmatrix} \widetilde{u}_1^1 & \widetilde{u}_1^2 & \cdots & \widetilde{u}_1^l \\ \widetilde{u}_2^1 & \widetilde{u}_2^2 & \cdots & \widetilde{u}_2^l \\ \cdots & \cdots & \cdots & \cdots \\ \widetilde{u}_n^1 & \widetilde{u}_n^2 & \cdots & \widetilde{u}_n^l \end{bmatrix}_{n\times l} \tag{15}$$

where $\widetilde{u}_j^i$ is the velocity at the j-th measurement point in the i-th experimental measurement ensemble, which includes synthetic experimental noise.

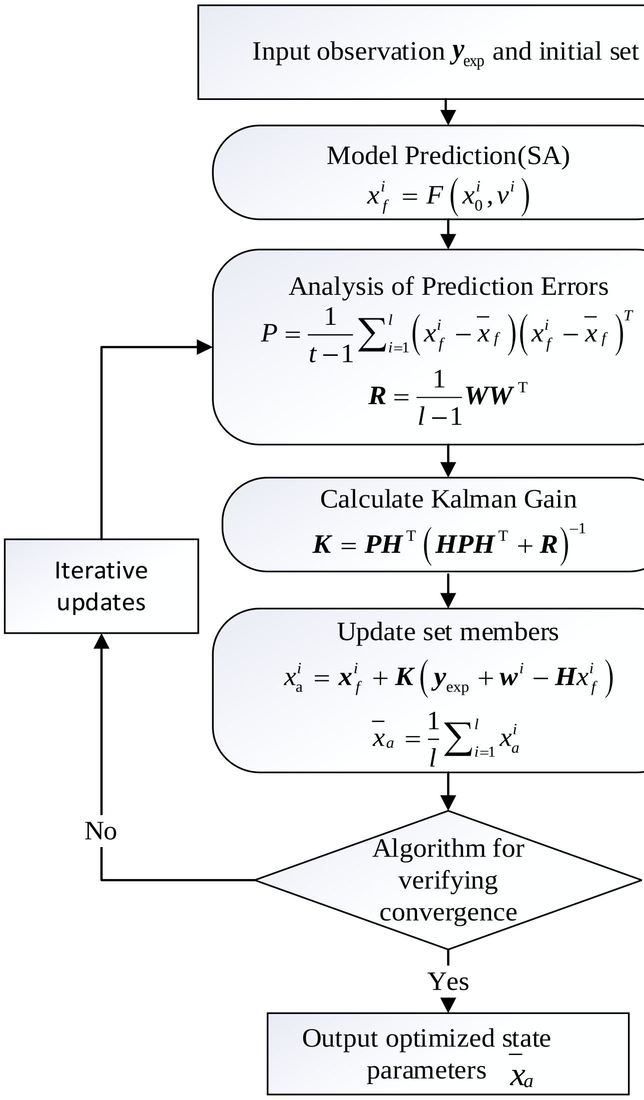

Figure 1. Turbulence model constant calibration process based on experimental data assimilation.

Based on the matrix forms of X and Y, the observation function matrix H is given by the following:

$$H_{n\times k} = \begin{pmatrix} I_n & 0_{n\times(k-n)} \end{pmatrix} \tag{16}$$

where $1_{M\times N}$ is a matrix of all ones in its elements, I_n is an identity matrix of order, $0_{m\times n}$ is a matrix of all zeros in its elements, matrix $1_{M\times N}$ is an M × N matrix with all elements equal to 1, matrix I_N is an N × N identity matrix, matrix $0_{M\times N}$ is an M × N matrix with all elements equal to 0, and the predicted element values at the points corresponding to the measurement locations are set to 1. Once the matrices X, Y, and H are determined, assimilation can be performed using the analysis and confirmation steps in EnKF to obtain the optimal constants for the RANS model.

The process for calibrating the turbulence model constants is illustrated in Figure 2. The calibration process first generates 100 sets of turbulence model constant samples using Latin Hypercubic Sampling (LHS) [31] and computes the velocity at the pipe centerline under different constant sample conditions by inputting them into the SA turbulence model, resulting in 100 sets of predicted velocities. The predicted velocities and the initial state matrix of the algorithm are integrated according to Equation (13). Subsequently, by combining the velocity observation data obtained from the experiment under the corresponding conditions and inputting them together into the Ensemble Kalman filtering algorithm, the optimal model constants for the observed data calibration can be obtained after multiple iterations of the analysis step. Finally, the calibrated constants are applied to recalculate under the same conditions to evaluate the reliability and applicability of the turbulence model constants.

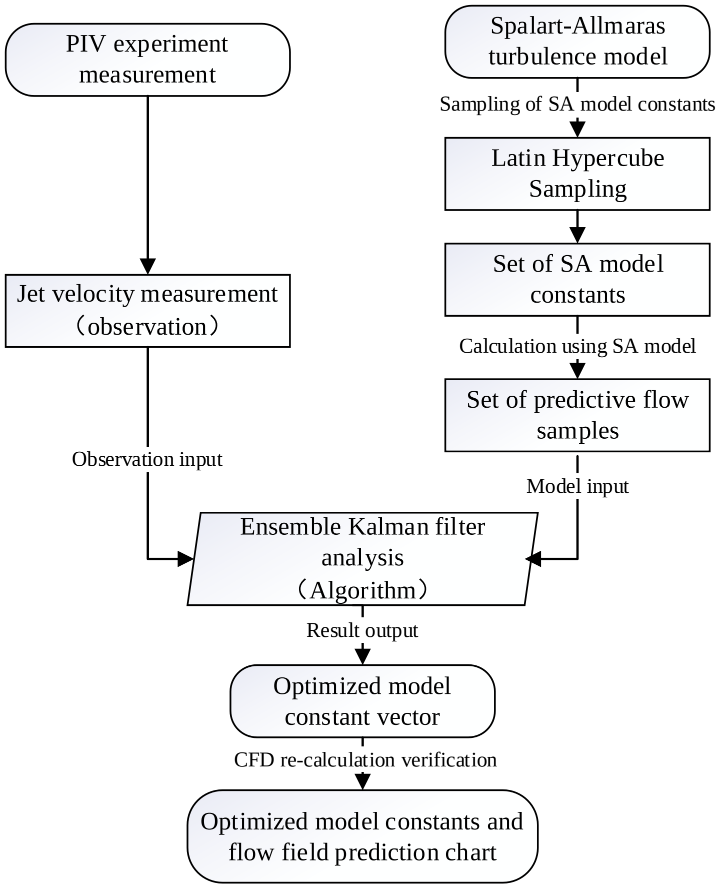

Figure 2. Calibration process of turbulence model constants based on experimental data.

3. Computational Example

3.1. Research Object

To investigate the flow characteristics of subsonic jet flows, this study selected an axisymmetric subsonic nozzle model with a Mach number of 0.51, namely the ARN2 nozzle shown in Figure 3. The ARN2 nozzle belongs to the convergent–divergent nozzle series and serves as an acoustic reference nozzle, which partially reflects the flow characteristics of subsonic jet flows. The ARN2 nozzle has an inlet diameter of 152.4 mm, a throat thickness of 1.27 mm, an outer surface angle of 30° with respect to the jet axis, and a parallel flow section of 6.4 mm at the exit. The NASA official website provides experimental velocity data downstream of the jet flow measured using Particle Image Velocimetry (PIV) for a Mach number of 0.51 M axisymmetric subsonic jet flow case [32], which serves as the velocity measurement data in this study. In order to verify the applicability of the assimilated turbulence model for velocity prediction of such jets, a validated case of axisymmetric heated subsonic jet with a NASA exit Mach number of approximately 0.376 [33] is selected as a validation case to analyze the improvement in velocity prediction accuracy of the assimilated SA turbulence model for the jet flow.

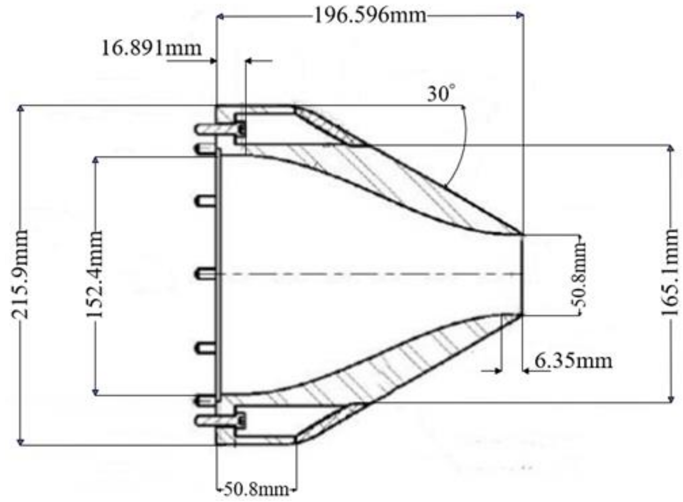

Figure 3. ARN2 Converging Nozzle.

3.2. Parameter Selection

In this study, the EnKF aims to estimate the constant values of the SA turbulence model. Therefore, the ordinary state variables of RANS are no longer applicable, and the model constants are added to the state variables to estimate the parameter values in Equation (12).

To ensure that the assimilation ensemble captures sufficient flow field variation information while maintaining the rationality of assimilation, the experimental observation data should fall within the range of the upper and lower limits of the predicted flow sample set. Therefore, the range of model parameter variations determined via perturbation analysis should be set at 50–150% of their original values (as shown in Figure 4), where X denotes the distance of the data extraction point along the horizontal axis from the nozzle, D denotes the diameter of the nozzle outlet, U denotes the velocity in the axial direction behind the nozzle, and U_j denotes the velocity at the nozzle outlet. Figure 4 shows that when the range is set between 50% and 150% of the original value, both the original prediction results of the SA model and the PIV experimental measurements fall within this range, satisfying the aforementioned conditions. Therefore, 100 sets of constant samples were extracted within this range using the Latin Hypercube Sampling (LHS) method [29]. The assimilation constants used in this study, along with their corresponding ranges, are as follows:

$$3.55 \leq c_{v1} \leq 10.65$$

$$0.06775 \leq c_{b1} \leq 0.20325$$

$$0.311 \leq c_{b2} \leq 0.933$$

$$0.15 \leq c_{w2} \leq 0.45$$

$$1 \leq c_{w3} \leq 3$$

3.3. Computational Settings

In this study, the ICEM 2020 R2 software was utilized to construct a two-dimensional model and generate a structured mesh. Since the nozzle under investigation is an axisymmetric nozzle, a symmetric structure was employed during the modeling process. The computational domain is illustrated in Figure 5, representing the fluid region for numerical simulations. The total length and width of the domain are 2.209 m and 1.524 m, respectively, with a total of 68,927 grid cells. To capture the turbulent characteristics of the jet core more accurately, the mesh was refined in the core region. The numerical simulations were conducted using the Finite Volume Method and the ANSYS Fluent 2020 R2 software [34,35], and the calculations were performed using a double-precision steady-state solver. Based on the information provided by NASA [32], a steady-state solution was calculated using the SA turbulence model. The working medium was an ideal gas, and the boundary conditions were set as follows: the inlet boundary conditions were $P_{in}/P_{ref} = 1.19671$ and $T_{in}/T_{ref} = 1$, where P_{in} and T_{in} are the total pressure and temperature at the inlet of the nozzle, respectively, and P_{ref} and T_{ref} are the ambient pressure and temperature, respectively, which were set to 101,325 Pa and 303.5 K. The outlet boundary condition was $P_{out}/P_{ref} = 1$, and the background environment condition was set to a Mach number of 0.01. To eliminate the influence of grid density and grid quantity on the computational results, numerical simulations were conducted using grid quantities of 70,000, 140,000, and 210,000, as shown in Figure 6. As the grid quantity increased, its impact on the numerical simulation was not significant. Therefore, in order to conserve computational resources, this study employed a grid quantity of approximately 70,000 for the simulation calculations until convergence was achieved. For the initial conditions, the default configuration of the standard initialization method in Fluent was utilized.

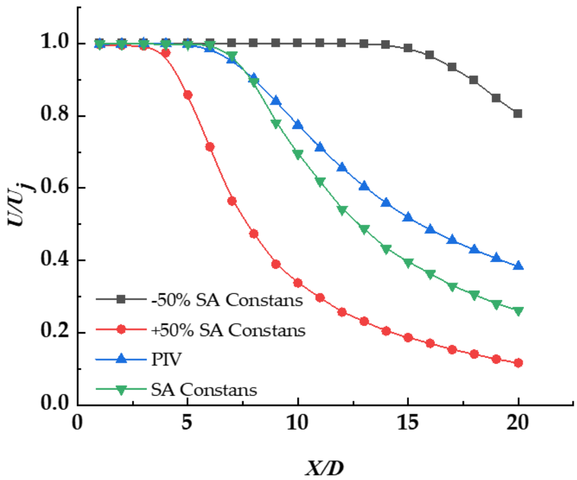

Figure 4. Range of model parameter changes.

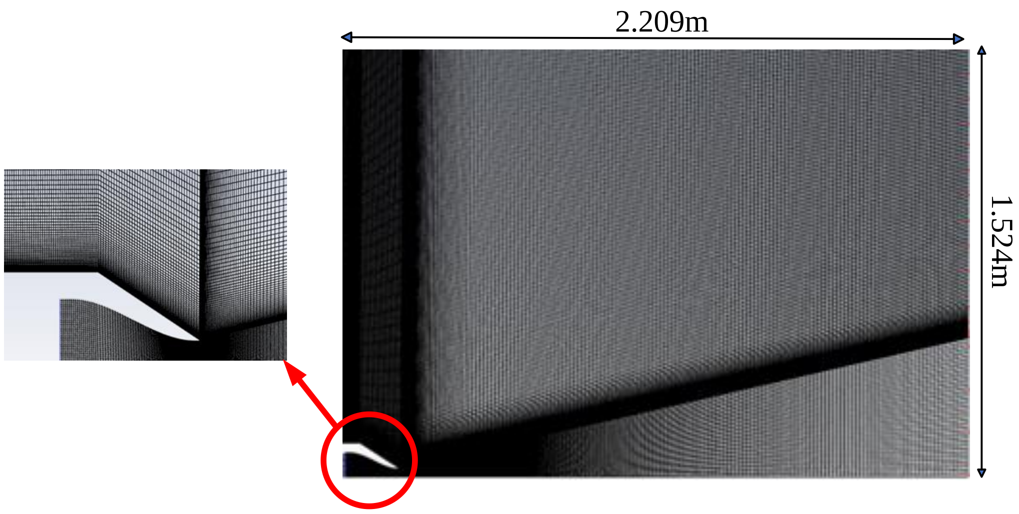

Figure 5. Nozzle structure mesh.

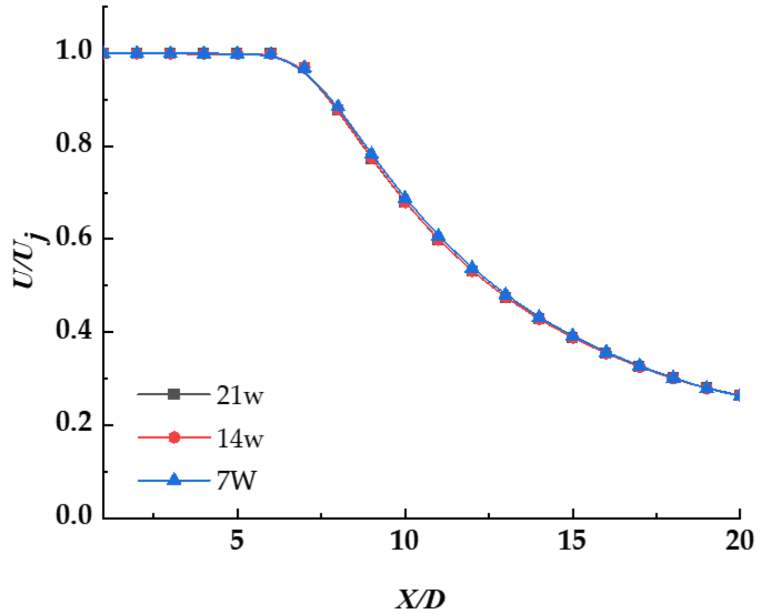

Figure 6. Grid independence validation.

4. Results and Discussions

In this study, the velocity of the jet flow in the region of 1 < X/D < 20 on the centerline of the flow, as measured using PIV experiments available on the NASA website, was selected as the observation data. Data from 20 measurement points evenly distributed along the axial direction were extracted, along with corresponding predicted data from the model, for assimilation.

4.1. Assimilation Results

First, the generated sample parameter set was input into the SA turbulent model for calculation, and the post-processing of the calculated results was performed using Tecplot software to obtain the initial sample prediction set. Figure 7 shows the dimensionless velocity contour distribution of the PIV and initial sample sets, where X represents the distance of the data extraction point in the horizontal axis direction to the nozzle, D represents the diameter of the nozzle outlet, U represents the velocity in the axial direction behind the nozzle, and U_j represents the velocity at the nozzle outlet. From Figure 6, it can be seen that the experimental measurement data is within the range of the predicted sample set, indicating that the generated initial sample set has captured sufficient flow field information and ensures the rationality of the assimilation.

Subsequently, the initial sample set and experimental measurement data were assimilated using the ensemble Kalman filter (EnKF) algorithm to obtain the assimilated model constants. Table 2 presents the original and assimilated constants of the SA turbulence model. The results show that after EnKF assimilation, some of the constants have undergone significant changes relative to their original values, while others have undergone relatively small changes. In particular, the constant c_{v1} increased by 50.7%, c_{b1} decreased by 6.6%, c_{b2} decreased by 56.5%, c_{w2} increased by 61.3%, and c_{w3} decreased by 41.5%.

The velocity contour maps obtained from PIV measurements, the original SA model, and the assimilated SA turbulence model are presented in Figure 8. Here, X represents the distance from the nozzle to the data extraction point in the horizontal direction, Y represents the distance from the nozzle to the data extraction point in the vertical direction, and D represents the diameter of the nozzle. As shown in Figure 8, the original SA model (Figure 8b) cannot accurately predict the jet flow measured via PIV (Figure 8a), especially in the region of 10 < X/D < 20 in the transition zone. However, the assimilated SA turbulence model, obtained by assimilating experimental data (Figure 8c), shows improved prediction accuracy for the jet flow. In the transition zone, the assimilated SA model demonstrates better agreement with both the original model and PIV measurement results, accurately predicting the velocity distribution in the core region of the jet, as well as the diffusion and decay regions.

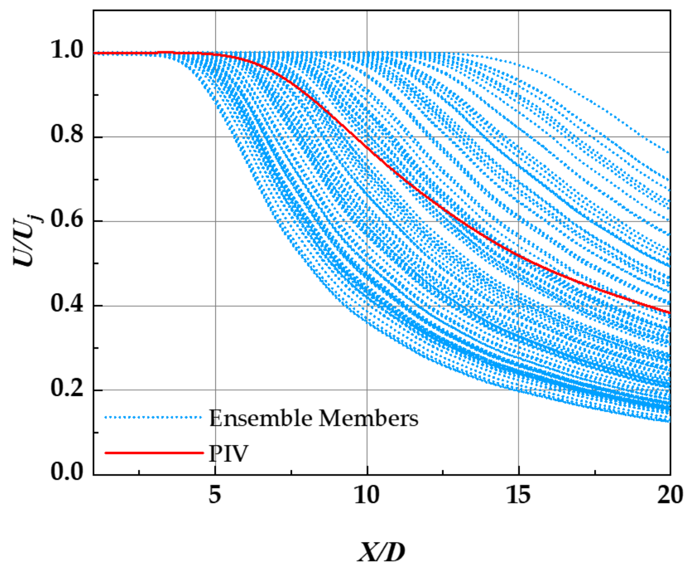

Figure 7. Distribution of initial sample prediction set and PIV experimental measurement.

Table 2. Comparison of original and optimized values of SA model constants.

Constants	c_{v1}	c_{b1}	c_{b2}	c_{w2}	c_{w3}
Original Value	7.1	0.1355	0.622	0.3	2.0
Optimized Value	10.7	0.126	0.269	0.484	1.16

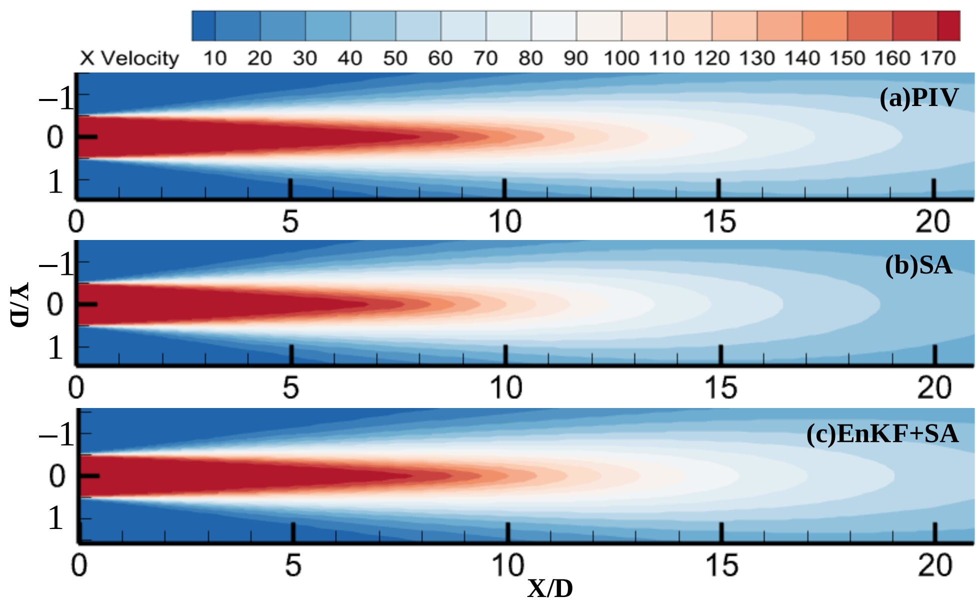

Figure 8. Velocity cloud maps of SA model before and after assimilation.

To comprehensively investigate the improvement effect of experimental data assimilation on the SA model, we selected typical areas in the horizontal and vertical directions behind the nozzle for analysis.

4.2. Analysis of Horizontal Direction Assimilation Effect

The analysis of the horizontal direction assimilation effect was conducted by selecting the data in the horizontal axis behind the nozzle in the range of Y/D = 0 and 0 < X/D < 20, as shown in Figure 9. The comparison between the PIV measurement and the results indicates that the original SA model fails to accurately predict the velocity distribution of the jet flow (Figure 9a). However, by employing the data assimilation technique of Ensemble Kalman Filter (EnKF) to enhance the SA model, significant improvements in the consistency between the EnKF-enhanced SA model and the experimental measurements obtained from PIV were observed compared to the original model. This enhanced SA model with EnKF demonstrated a more accurate prediction of jet diffusion and decay (Figure 9b). Specifically, a noticeable enhancement in the predictive accuracy of the turbulent model was observed in the region of 10 < X/D < 20 after data assimilation. These findings highlight the capability of data assimilation techniques in improving the predictive accuracy of turbulent models.

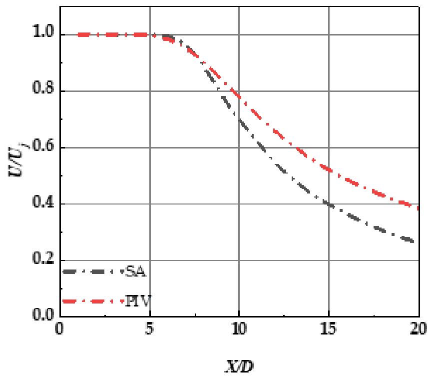

(**a**)

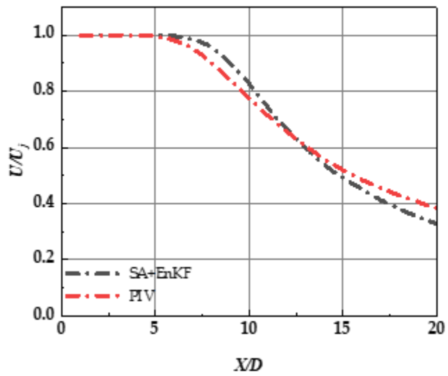

(**b**)

Figure 9. (**a**) Horizontal axial velocity curve before assimilation of SA model; (**b**) horizontal axial velocity curve after assimilation of SA model.

Figure 10 shows the relative errors between the predicted jet velocity via the SA model before and after data assimilation and the PIV measurements. The relative error is defined as follows:

$$Error = \frac{|U^* - U_{piv}|}{U_{piv}} \tag{17}$$

where U_{piv} is the PIV experimental measurement velocity at the measurement point, and U^* is the model predicted velocity at the experimental data position. As shown in Figure 10, in the original SA model, as the distance from the nozzle increases and the jet velocity decays, the prediction error downstream of the nozzle gradually increases, with an overall spatial relative error of 13.04%. However, the relative error produced via the SA model with optimized constants after assimilation is smaller as the velocity decays, with an overall spatial relative error of only 4.6%.

4.3. Analysis of Vertical Direction Assimilation Effect

After data assimilation, the SA turbulence model exhibits improved numerical predictions of the vertical flow field, as shown in Figure 11a–d. At distances X/D = 5, 10, 15, and 20 downstream of the nozzle, 20 uniformly distributed velocity measurement points were selected for analysis along the vertical direction 0 < Y/D< 1.4. It was found that both the standard SA model and the assimilated SA model accurately predicted the velocity distribution at X/D = 5. However, as the distance from the nozzle increased, the error of the two models also gradually increased at X/D = 10, 15, and 20, in line with the tendency for the prediction error of the model to increase with the attenuation of the velocity in the horizontal direction of the nozzle axis. Nonetheless, overall, the assimilated SA model exhibits better prediction accuracy than the original SA model at X/D = 10, 15, and 20.

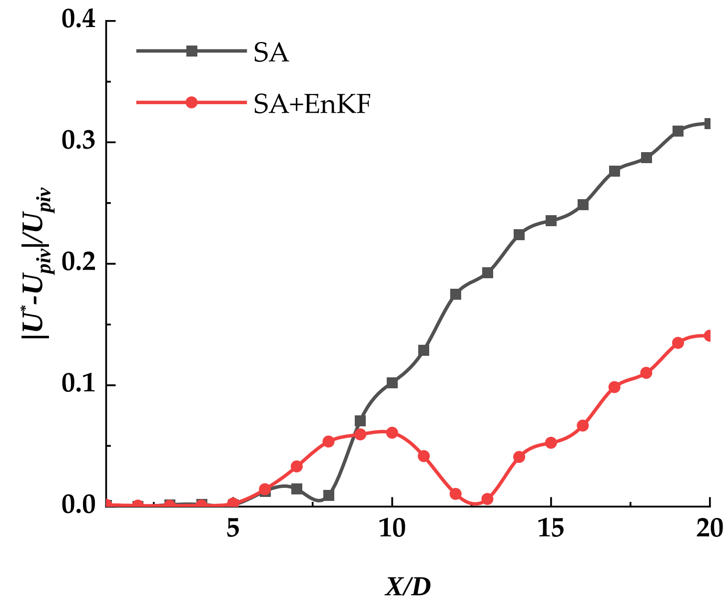

Figure 10. Relative error of SA model before and after assimilation.

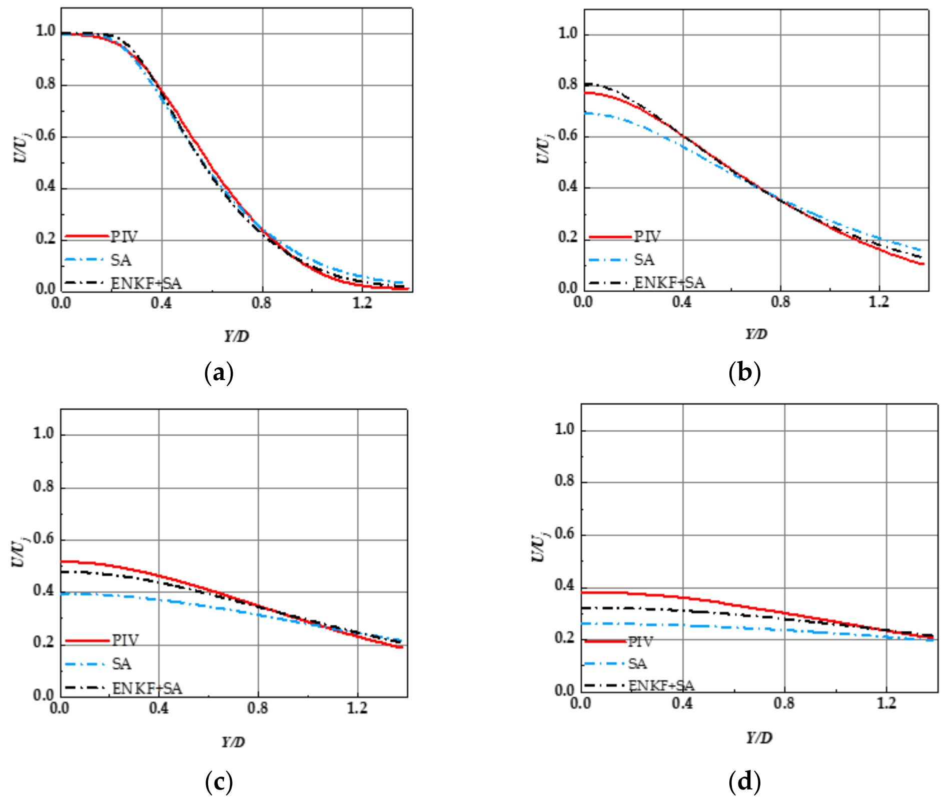

Figure 11. Dimensionless velocity curves before and after assimilation of the SA model: (**a**) X/D = 5, (**b**) X/D = 10, (**c**) X/D = 15, and (**d**) X/D = 20.

Therefore, the data assimilation-based turbulent model exhibits an improvement in the accuracy of velocity numerical predictions across the entire flow field space.

Figure 12 shows the relative errors between the predicted jet velocities via the SA model before and after data assimilation and the PIV experimental data at four vertical positions. In the original SA model, the relative errors at X/D = 5, 10, 15, and 20 are 39.2%, 12.6%, 13.6%, and 21.9%, respectively. In contrast, in the EnKF assimilated SA model, the corresponding relative errors are 18.2%, 4.5%, 4.9%, and 8.9%, respectively. Additionally, it can be seen from Figure 12 that as the distance from the nozzle increases, the errors at Y/D = 0 also increase. Nevertheless, the assimilated SA model consistently exhibits higher accuracy in predicting the jet velocity in the vertical direction than the original SA model.

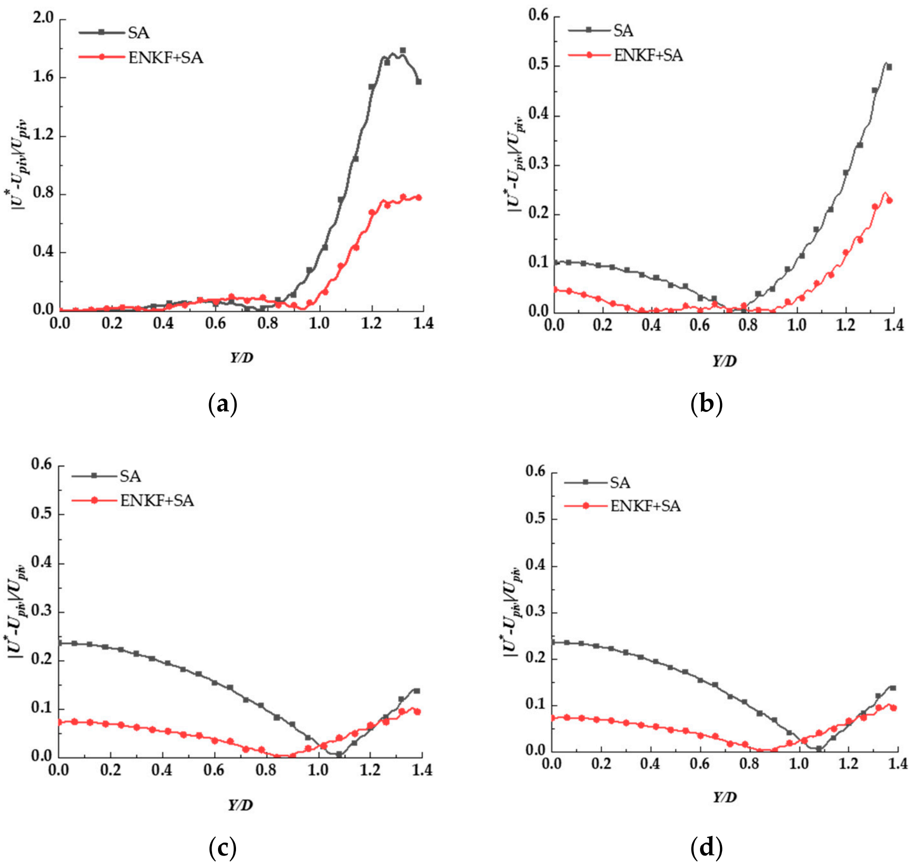

Figure 12. Relative errors in the vertical direction before and after assimilation of the SA model: (**a**) X/D = 5, (**b**) X/D = 10, (**c**) X/D = 15, and (**d**) X/D = 20.

4.4. Analysis of Assimilation Effects on Jet Flow under Different Conditions

The NASA axisymmetric hypersonic jet flow case [33] was selected to validate the improved accuracy of the assimilated SA turbulence model under various flow states. Based on the information provided by NASA, the ARN2 nozzle was used in this case, and the computational domain and settings remained consistent with the previous description. The simulation was conducted in steady-state mode using the SA turbulence model as the baseline model, with an ideal gas selected as the working medium. The boundary conditions were defined as follows: the inlet boundary conditions were set as $P_{in}/P_{ref} = 1.10203$ and $T_{in}/T_{ref} = 1.81388$, where P_{in} and T_{in} represent the total pressure and total temperature at the nozzle inlet, and P_{ref} and T_{ref} represent the actual external environmental conditions, with values of 101,325 Pa and 295 K, respectively. The outlet boundary condition was set as $P_{out}/P_{ref} = 1$, and the background ambient condition was set to a Mach number of $M = 0.01$. Other settings were the same as in the previous case. The analysis focused on the uniformly distributed velocity data in the downstream horizontal axis direction at Y/D = 0. As shown in Figures 13 and 14, it can be observed that the velocity prediction performance of the SA turbulence model improved after data assimilation. The model constants, modified via assimilation with experimental data, demonstrated better adaptability to the flow characteristics of the hypersonic jet. The spatial relative error of velocity prediction via the standard SA turbulence model prior to assimilation was 13.7%. However, the SA turbulence model with optimized constants achieved a significantly reduced spatial relative error of only 5.5%. These results clearly indicate that the turbulence model constants, modified via data assimilation, are more suitable for predicting jet flow compared to their original values.

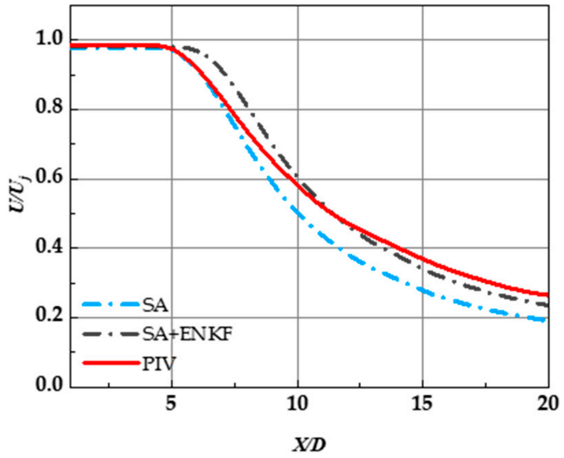

Figure 13. Effect of recalibrated turbulence model constants on simulation and prediction of hypersonic jet flow.

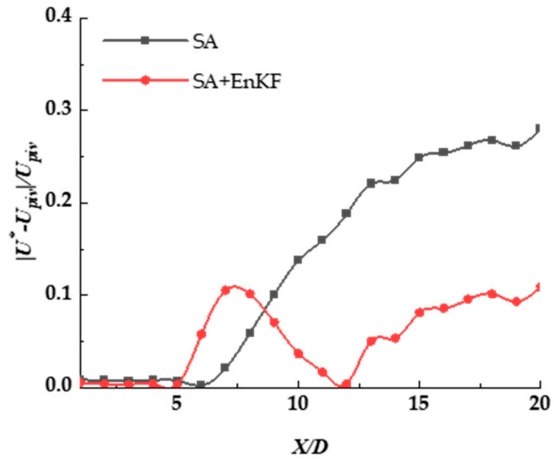

Figure 14. Analysis of relative error in simulation and prediction of hypersonic jet flow via SA model before and after data assimilation.

5. Conclusions

In this paper, the data assimilation method is used, with NASA's PIV experimental measurement as the observation data and the ensemble Kalman filter algorithm as the assimilation algorithm to recalibrate the constants of the SA model and optimize the accuracy of the numerical prediction of subsonic jet flow. The main conclusions obtained are listed as follows:

(1) The assimilation results demonstrate the suitability of this approach for the optimization of turbulence model constants. In particular, the SA model with EnKF assimilation can effectively conduct numerical simulations of jet flow via a nozzle by optimizing the model constants while keeping the model structure unchanged.
(2) According to the numerical simulation results using the EnKF assimilated SA model, the average relative error in the horizontal direction (Y/D = 0) significantly decreased from 13.04% to 4.6% in the original case. In the vertical direction at X/D = 5, 10, 15, and 20, the average relative errors reduced from 39.2%, 12.6%, 13.6%, and 21.9% to 18.2%, 4.5%, 4.9%, and 8.9%, respectively. In the validation case, the standard SA turbulence model exhibited a spatial relative error of 13.7% in predicting the velocity of the thermal subsonic jet flow, while the SA model with optimized constants achieved a

significantly reduced spatial relative error of 5.5%. These findings demonstrate that the turbulence model constants, calibrated via data assimilation, are better suited for predicting jet flow compared to their original values.

(3) From this paper, it can be seen that the turbulence model correction method in this paper has two major advantages. First, this method uses data assimilation methods, which are data-driven model constant optimization methods that can fully utilize observation data; at the same time, the Ensemble Kalman filter algorithm used in this paper can comprehensively consider the errors existing in model prediction and experimental observation, thereby giving more accurate estimates and more practical results.

(4) The assimilated turbulent model has significantly improved the accuracy of numerical simulations for subsonic jet flows, providing valuable insights for the optimization of numerical simulations for subsonic nozzle flows. The findings of this study are of great importance in determining the safety clearance behind the takeoff point under the influence of jet flows from aircraft engines. By defining the extent of the jet flow influence from the preceding aircraft and determining the crossing interval for the subsequent aircraft, airport operational efficiency can be enhanced, leading to reduced takeoff spacing, optimized flight scheduling and management, and improved overall efficiency and sustainability of airport operations.

This study only considers the assimilation impact of the SA turbulence model on jet flows and specifically investigates the jet characteristics under different conditions with the same nozzle geometry. In the future, the influence of data assimilation on numerical simulations can be explored from multiple dimensions, such as other turbulence models, different assimilation algorithms, and additional variables in experiments.

Author Contributions: Conceptualization, H.G. and C.Y.; methodology, X.H. and Y.C.; software, C.Y.; validation, X.H., H.G. and C.Y.; formal analysis, X.H. and Y.C.; investigation, X.H., H.G. and R.Z.; resources, X.H. and Y.C.; data curation, X.H. and C.Y.; writing—original draft preparation, C.Y. and R.Z.; writing—review and editing, X.H. and C.Y.; visualization, X.H. and C.Y.; supervision, X.H.; project administration, Y.C.; funding acquisition, Y.C. All authors have read and agreed to the published version of the manuscript.

Funding: This research was funded by the Civil Aviation Administration of China Security Capability Project: Study on Safety Separation Interval for Aircraft Operations Behind Jet Blast Effects During Takeoff, No. [2022] 186, Research and Innovation Team of Civil Aviation Flight Academy of China: Flight Efficiency Improvement Research Center, Institution No. CZKY2023156.

Institutional Review Board Statement: Not applicable.

Informed Consent Statement: Not applicable.

Data Availability Statement: The datasets generated during and/or analyzed during this current study are available from the corresponding author upon reasonable request.

Conflicts of Interest: The authors declare no conflict of interest.

References

1. Chen, Y.Q.; Zhang, X.Y. A Preliminary study on schemes on crossing runway behind takeoff aircraft at the Chongqing Jiangbei airport. *J. Civ. Aviat. Viation* **2018**, *2*, 25–30.
2. Uzun, A.; Hussaini, M.Y. Prediction of noise generated by a round nozzle jet flow using computational aeroacoustics. *J. Comput. Acoust.* **2011**, *19*, 291–316. [CrossRef]
3. Xie, J.L.; Zhong, X.P.; Wang, J.B. Experimental and numerical simulation of subsonic jet flow. *J. Eng. Thermophys.* **2013**, *34*, 1457–1461.
4. Manovski, P.; Novara, M.; Mohan, N.K.D.; Geisler, R.; Schanz, D.; Agocs, J.; Godbersen, P.; Schröder, A. 3D Lagrangian particle tracking of a subsonic jet using multi-pulse Shake-The-Box. *Exp. Therm. Fluid Sci.* **2021**, *123*, 110346. [CrossRef]
5. Yang, Y.; Wang, G.; Shi, W.; Li, W.; Ji, L.; Wang, H. Turbulence Characteristics in the Mixing Layer of a Submerged Cavitating Jet at High Reynolds Numbers. *Sustainability* **2022**, *14*, 11963. [CrossRef]
6. Zhang, Q.; Shi, Z.; Shi, W.; Xie, Z.; Tan, L.; Yang, Y. Research on Flow Field Characteristics in Water Jet Nozzle and Surface Damage Caused by Target Impact. *Sustainability* **2022**, *14*, 9074. [CrossRef]

7. He, X.; Hu, D.F.; Liu, C.; Ma, Y.L. Study on Improving the Distance of Engine Jet Influence using DES Method and SA Model. *Chin. J. Saf. Sci.* **2021**, *31*, 81–87. [CrossRef]
8. Duraisamy, K.; Iaccarino, G.; Xiao, H. Turbulence modeling in the age of data. *Annu. Rev. Fluid Mech.* **2019**, *51*, 357–377. [CrossRef]
9. Xiao, H.; Cinnella, P. Quantification of model uncertainty in RANS simulations: A review. *Prog. Aerosp. Sci.* **2019**, *108*, 1–31. [CrossRef]
10. He, C.X.; Deng, Z.W.; Liu, Y.Z. Turbulent flow data assimilation technology and its application. *J. Aeronaut.* **2021**, *42*, 524704.
11. Ma, J.W.; Qin, S.X. A review of data assimilation algorithms. *Adv. Earth Sci.* **2012**, *27*, 747–757.
12. Margheri, L.; Meldi, M.; Salvetti, M.; Sagaut, P. Epistemic uncertainties in RANS model free coefficients. *Comput. Fluids* **2014**, *102*, 315–335. [CrossRef]
13. Kato, H.; Yoshizawa, A.; Ueno, G.; Obayashi, S. A data assimilation methodology for reconstructing turbulent flows around aircraft. *J. Comput. Phys.* **2015**, *283*, 559–581. [CrossRef]
14. Zhang, X.L.; Michelén-Ströfer, C.; Xiao, H. Regularized ensemble Kalman methods for inverse problems. *J. Comput. Phys.* **2020**, *416*, 109517. [CrossRef]
15. Li, Z.; Zhang, H.; Bailey, S.C.; Hoagg, J.B.; Martin, A. A data-driven adaptive Reynolds-averaged Navier–Stokes k–ω model for turbulent flow. *J. Comput. Phys.* **2017**, *345*, 111–131. [CrossRef]
16. Gallo, L.A.; Chica, E.L.; Flórez, E.G. Numerical Optimization of the Blade Profile of a Savonius Type Rotor Using the Response Surface Methodology. *Sustainability* **2022**, *14*, 5596. [CrossRef]
17. Mi, H.; Wang, C.; Jia, X.; Hu, B.; Wang, H.; Wang, H.; Zhu, Y. Hydraulic Characteristics of Continuous Submerged Jet Impinging on a Wall by Using Numerical Simulation and PIV Experiment. *Sustainability* **2023**, *15*, 5159. [CrossRef]
18. Deng, Z.; He, C.; Wen, X.; Liu, Y. Recovering turbulent flow field from local quantity measurement: Turbulence modeling using ensemble-Kalman-filter-based data assimilation. *J. Vis.* **2018**, *21*, 1043–1063. [CrossRef]
19. Elsinga, G.E.; Scarano, F.; Wieneke, B.; van Oudheusden, B.W. Tomographic particle image velocimetry. *Exp. Fluids* **2006**, *41*, 933–947. [CrossRef]
20. Raffel, M.; Willert, C.; Kompenhans, J. *Particle Image Velocimetry: A Practical Guide*; Springer: Göttingen, Germany, 1998.
21. Spalart, P.; Allmaras, S. In A one-equation turbulence model for aerodynamic flows. In Proceedings of the 30th Aerospace Sciences Meeting and Exhibit, Reno, NV, USA, 6–9 January 1992; p. 439. [CrossRef]
22. Le Dimet, F.-X.; Talagrand, O. Variational algorithms for analysis and assimilation of meteorological observations: Theoretical aspects. *Tellus A Dyn. Meteorol. Oceanogr.* **1986**, *38*, 97–110. [CrossRef]
23. Evensen, G. Sequential data assimilation with a nonlinear quasi-geostrophic model using Monte Carlo methods to forecast error statistics. *J. Geophys. Res. Ocean.* **1994**, *99*, 10143–10162. [CrossRef]
24. Kato, H.; Obayashi, S. In Data assimilation for turbulent flows. In Proceedings of the 16th AIAA Non-Deterministic Approaches Conference, National Harbor, MD, USA, 13–17 January 2014; p. 1177. [CrossRef]
25. Meinhold, R.J.; Singpurwalla, N.D. Understanding the Kalman filter. *Am. Stat.* **1983**, *37*, 123–127.
26. Grewal, M.S.; Andrews, A.P.; Bartone, C.G. *Kalman Filtering*; Wiley Telecom: Göttingen, Germany, 2020; pp. 355–417.
27. Houtekamer, P.L.; Mitchell, H.L. Data assimilation using an ensemble Kalman filter technique. *Mon. Weather Rev.* **1998**, *126*, 796–811. [CrossRef]
28. Evensen, G. *Data Assimilation: The Ensemble Kalman Filter*; Springer: Berlin, Germany, 2009; Volume 2.
29. Kato, H.; Obayashi, S. Approach for uncertainty of turbulence modeling based on data assimilation technique. *Comput. Fluids* **2013**, *85*, 2–7. [CrossRef]
30. Fang, P.; He, C.; Xu, S.W.P.; Liu, Y. Turbulence Model Constant Calibration based on Experimental Data Assimilation: Numerical Prediction of Flow Characteristics in Steam Valve with Filter. *J. Aerodyn.* **2021**, *39*, 12–22.
31. Olsson, A.; Sandberg, G.; Dahlblom, O. On Latin hypercube sampling for structural reliability analysis. *Struct. Saf.* **2003**, *25*, 47–68. [CrossRef]
32. NASA. Langley Research Center Turbulence Modeling Resource: Axisymmetric Subsonic Jet. Available online: https://turbmodels.larc.nasa.gov/jetsubsonic_val.html (accessed on 5 December 2022).
33. NASA. Langley Research Center Turbulence Modeling Resource: Axisymmetric Hot Subsonic Jet. Available online: https://turbmodels.larc.nasa.gov/jetsubsonichot_val.html (accessed on 5 January 2023).
34. Yang, S.; Ai, Z.; Zhang, C.; Dong, S.; Ouyang, X.; Liu, R.; Zhang, P. Study on Optimization of Tunnel Ventilation Flow Field in Long Tunnel Based on CFD Computer Simulation Technology. *Sustainability* **2022**, *14*, 11486. [CrossRef]
35. Alwafi, A.M.; Alshehri, S.M.; Alzahrani, S.M. Computational Fluid Dynamics Modeling of Single Isothermal and Non-Isothermal Impinging Jets in a Scaled-Down High-Temperature Gas-Cooled Reactor Facility. *Processes* **2023**, *11*, 46. [CrossRef]